

Open Wilson chains for quantum impurity models: Keeping track of all bath modes

B. Bruognolo,^{1,2} N.-O. Linden,¹ F. Schwarz,¹ S.-S. B. Lee,¹ K. Stadler,¹ A. Weichselbaum,¹
M. Vojta,³ F. B. Anders,⁴ and J. von Delft¹

¹*Physics Department, Arnold Sommerfeld Center for Theoretical Physics and Center for NanoScience,
Ludwig-Maximilians-Universität München, D-80333 München, Germany*

²*Max-Planck-Institut für Quantenoptik, Hans-Kopfermann-Strasse 1, D-85748 Garching, Germany*

³*Institut für Theoretische Physik, Technische Universität Dresden, D-01062 Dresden, Germany*

⁴*Lehrstuhl für Theoretische Physik II, Technische Universität Dortmund, D-44221 Dortmund, Germany*

(Received 22 November 2016; published 31 March 2017)

When constructing a Wilson chain to represent a quantum impurity model, the effects of truncated bath modes are neglected. We show that their influence can be kept track of systematically by constructing an “open Wilson chain” in which each site is coupled to a separate effective bath of its own. As a first application, we use the method to cure the so-called mass-flow problem that can arise when using standard Wilson chains to treat impurity models with asymmetric bath spectral functions at finite temperature. We demonstrate this for the strongly sub-Ohmic spin-boson model at quantum criticality where we directly observe the flow towards a Gaussian critical fixed point.

DOI: [10.1103/PhysRevB.95.121115](https://doi.org/10.1103/PhysRevB.95.121115)

A quantum impurity model describes a discrete set of degrees of freedom, the “impurity”, coupled to a bath of excitations. For an infinite bath this is effectively an *open* system. However, the most powerful numerical methods for solving such models, Wilson’s numerical renormalization group (NRG) [1,2] and variational matrix-product-state (VMPS) generalizations thereof [3–6], actually treat it as *closed*: The continuous bath is replaced by a so-called Wilson chain, a finite-length tight-binding chain whose hopping matrix elements t_n decrease exponentially with site number n , ensuring energy-scale separation along the chain. This works well for numerous applications, ranging from transport through nanostructures [7,8] to impurity solvers for dynamical mean-field theory [9–11]. However, replacing an open by a closed system brings about finite-size effects. Wilson himself had anticipated that the effect of bath modes neglected during discretization might need to be included perturbatively “to achieve reasonable accuracy”, but concluded that “this has proven to be unnecessary” for his purposes (see p. 813 of Ref. [1]). By now, it is understood that finite-size effects often do matter. They hamper the treatment of dissipative effects [12], e.g., in the context of nonequilibrium transport [13] and equilibration after a local quench [14]. Moreover, even in equilibrium, they may cause errors when computing the bath-induced renormalization of impurity properties [15–17]. Indeed, finite-size issues constitute arguably the most serious conceptual limitation of approaches based on Wilson chains.

Here, we set the stage for controlling finite-size effects by constructing “open Wilson chains” (OWCs) in which each site is coupled to a bath of its own. The resulting open system implements energy-scale separation in a way that, in contrast to standard Wilson chains (SWCs), fully keeps track of all bath-induced dissipative and renormalization effects. The key step involved in any renormalization group (RG) approach, namely, integrating out degrees of freedom at one energy scale to obtain a renormalized description at a lower scale, can then be performed more carefully than for SWCs. We illustrate this by focusing on renormalization effects, leaving a systematic treatment of dissipative effects on OWCs for the future.

A SWC is constructed by logarithmically discretizing the bath and tridiagonalizing the resulting discrete bath Hamiltonian to obtain a tight-binding chain, with the impurity coupled to site $n = 0$ [1,2]. Properties at temperature T are calculated using a chain of finite length N_T , chosen such that its smallest energy scale matches the temperature $t_{N_T} \simeq T$ ($k_B = 1$). However, since sites $n > N_T$ are neglected, the contribution of the corresponding truncated bath modes (TBMs) to the renormalization of impurity properties is missing [17]. For example, for a local level linearly coupled to a bath with an asymmetric bath spectrum, this coupling generates a physical shift in the level energy. When this shift is computed using a SWC of length N_T , the result contains a temperature-dependent error. Hence, the use of SWCs generically leads to qualitative errors in the temperature dependence of renormalized model parameters, called the “mass-flow problem” [16,17]. Quantitative errors persist even for $T \rightarrow 0$, when $N_T \rightarrow \infty$, because constructing a SWC actually involves neglecting TBMs at *every* site.

The mass-flow problem is particularly serious when targeting a quantum critical point, where it causes errors for critical exponents describing finite-temperature properties at the critical point. This has been studied in some detail for the dissipative harmonic oscillator (DHO) and the sub-Ohmic spin-boson model (SBM). For both, SWCs are unable to even qualitatively describe the temperature dependence of the local susceptibility $\chi(T)$ at criticality [15–17]. Both involve Gaussian criticality of ϕ^4 type and hence a bosonic mode whose excitation energy vanishes at the critical fixed point. The finite-temperature RG flow in its vicinity cannot be correctly described using finite-length SWCs because the erroneous mass dominates over physical interaction effects. Summarizing, methods based on SWCs produce systematic quantitative errors for all impurity problems with asymmetric baths, and they fail even qualitatively in addressing Gaussian criticality and other phenomena with zero modes.

Here, we show that these issues *can* be addressed using OWCs: The bath coupled to each site of the OWC induces an energy shift for that site that can be computed *exactly* and

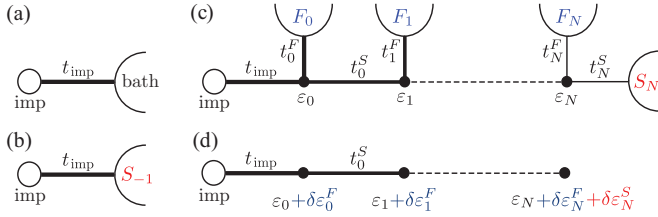


FIG. 1. (a) Impurity model. (b) Initialization. (c) Open Wilson chain (OWC). (d) Renormalized Wilson chain (RWC).

used to define a “renormalized Wilson chain” (RWC). The ground-state properties of a RWC of length N_T mimic the finite- T properties of the original model in a way that is free from mass-flow problems. We demonstrate this explicitly by using VMPS techniques [6] on RWCs to compute $\chi(T)$ for the DHO and SBM. We also compute the energy-level flow of the SBM; it unambiguously reveals flow towards a Gaussian fixed point with a dangerously irrelevant interaction term.

Model. We consider a generic single-band impurity model with Hamiltonian $\mathcal{H} = \mathcal{H}^{\text{imp}}[b^\dagger t_{\text{imp}}] + \mathcal{H}^{\text{bath}}$, where $\mathcal{H}^{\text{bath}}$ describes the bath, and \mathcal{H}^{imp} the impurity and its coupling to the bath via normalized bath operators b^\dagger and b , with coupling constant t_{imp} [Fig. 1(a)]. The free ($t_{\text{imp}} = 0$) dynamics of b^\dagger , generated by $\mathcal{H}^{\text{bath}}$, is encoded in the free retarded correlator $\mathcal{G}^{\text{bath}}(\omega) = \langle\langle b|b^\dagger \rangle\rangle_\omega$, which is uniquely characterized by its spectral function $\mathcal{A}^{\text{bath}}(\omega) = -\frac{1}{\pi} \text{Im} \mathcal{G}^{\text{bath}}(\omega)$. The impurity dynamics is therefore fully determined once \mathcal{H}^{imp} and the “bath spectrum”, $\Gamma^{\text{bath}}(\omega) = |t_{\text{imp}}|^2 \mathcal{A}^{\text{bath}}(\omega)$, have been specified.

Continued-fraction expansion. One well-known way of mapping an impurity model to a chain is to iteratively construct a continued-fraction expansion (CFE) for $\mathcal{G}^{\text{bath}}$ [18]. Our main idea is to do this in a way that *zooms in on low energies* without discarding high-energy information. Our construction involves a sequence of retarded correlators $\mathcal{G}_n^X(\omega)$, with $X = S$ or F , describing the effective “slow” (low-energy) or “fast” (high-energy) bath modes of iteration step n , with spectral functions $\mathcal{A}_n^X(\omega) = -\frac{1}{\pi} \text{Im} \mathcal{G}_n^X(\omega)$ having unit weight $\int d\omega \mathcal{A}_n^X(\omega) = 1$. We initialize our CFE construction with $\mathcal{G}_{-1}^S = \mathcal{G}^{\text{bath}}$ [Fig. 1(b)]. Starting with $n = 0$, we iteratively use \mathcal{G}_{n-1}^S , describing the low-energy modes of the previous iteration, as input to define a new retarded correlator \mathcal{G}_n and its retarded self-energy Σ_n ,

$$\mathcal{G}_n(\omega) = \mathcal{G}_{n-1}^S(\omega) = 1/[\omega - \varepsilon_n - \Sigma_n(\omega)], \quad (1)$$

with $\varepsilon_n = \int d\omega \omega \mathcal{A}_n(\omega)$ [19]. Then we split this self-energy into low- and high-energy parts by writing it as

$$\Sigma_n(\omega) = \Sigma_n^S(\omega) + \Sigma_n^F(\omega), \quad \Sigma_n^X(\omega) = |t_n^X|^2 \mathcal{G}_n^X(\omega). \quad (2)$$

Here, the corresponding retarded correlators $\mathcal{G}_n^{S/F}$ are defined by choosing their rescaled spectral functions $|t_n^{S/F}|^2 \mathcal{A}_n^{S/F}$ to represent the low- and high-energy parts of $\Gamma_n(\omega) = -\frac{1}{\pi} \text{Im} \Sigma_n$, with t_n^X chosen such that \mathcal{A}_n^X has unit weight (see Sec. S-1 A of Ref. [19] for details). To be explicit, we write $\Gamma_n = \Gamma_n^S + \Gamma_n^F$, with $\Gamma_n^X(\omega) = w_n^X(\omega) \Gamma_n(\omega)$. The splitting functions $w_n^{S/F}(\omega)$ are defined on the support of Γ_n , take values in the interval $[0, 1]$, satisfy $w_n^S(\omega) + w_n^F(\omega) = 1$, and have weight predominantly at low/high energies. Then

we write the split bath spectra as $\Gamma_n^X(\omega) = |t_n^X|^2 \mathcal{A}_n^X(\omega)$, with “couplings” t_n^X chosen as $|t_n^X|^2 = \int d\omega \Gamma_n^X(\omega)$, and define new retarded correlators via $\mathcal{G}_n^X(\omega) = \int d\bar{\omega} \frac{\mathcal{A}_n^X(\bar{\omega})}{\omega - \bar{\omega} + i0^+}$, also fixing $\Sigma_n^X(\omega)$ via Eq. (2).

Iterating, using \mathcal{G}_n^S as input to compute new correlators \mathcal{G}_{n+1}^X while retaining the self-energy Σ_n^F , we obtain a sequence of exact CFE representations for $\mathcal{G}^{\text{bath}}$. That of depth 2, e.g., reads

$$\mathcal{G}^{\text{bath}}(\omega) = \frac{1}{\omega - \varepsilon_0 - \Sigma_0^F(\omega) - \frac{|t_0^S|^2}{\omega - \varepsilon_1 - \Sigma_1^F(\omega) - \frac{|t_1^S|^2}{\omega - \varepsilon_2 - \Sigma_2^F(\omega)}}}.$$

To ensure energy-scale separation, we choose $\mathcal{A}_n^X(\omega)$ such that the CFE parameters decrease monotonically, $\max\{|\varepsilon_n|, |t_n^S|\} \leq \max\{|\varepsilon_{n-1}|, |t_{n-1}^S|\}/\Lambda$, with $\Lambda > 1$ [20].

Open Wilson chain. We now use the CFE data $(\varepsilon_n, t_n^X, \mathcal{G}_n^X)$ to represent the original bath in terms of a chain with $N + 1$ sites, each coupled to a bath of its own, and site 0 coupled to the impurity (site -1) [Fig. 1(c)]. This OWC is constructed such that the free ($t_{\text{imp}} = 0$) correlator of site 0 is exactly equal to the depth- N CFE found above, i.e., $\mathcal{G}_0 = \mathcal{G}^{\text{bath}}$, implying that the chain and original bath have the same effect on the impurity.

The key point is that each CFE step of writing $\mathcal{G}_{n-1}^S(\omega)$ in the form $\mathcal{G}_n(\omega) = 1/[\omega - \varepsilon_n - \Sigma_n(\omega)]$ can be implemented on the level of the Hamiltonian: It corresponds to replacing the bath represented by \mathcal{G}_{n-1}^S , say, S_{n-1} , by a new site n , with energy ε_n and normalized site operators f_n^\dagger and f_n , which is linearly coupled to a new bath that generates the self-energy Σ_n . In the present case, the latter is split into low- and high-energy contributions, $\Sigma_n^S + \Sigma_n^F$. We can generate these by linearly coupling the new site with couplings t_n^S and t_n^F to two new baths, say, S_n and F_n , via normalized bath operators $b_{S_n}^\dagger, b_{S_n}$ and $b_{F_n}^\dagger, b_{F_n}$, that are governed by bath Hamiltonians \mathcal{H}_n^X chosen such that $\langle\langle b_{X_n} | b_{X_n}^\dagger \rangle\rangle_\omega$ equals the $\mathcal{G}_n^X(\omega)$ found above (see Sec. S-1 A of Ref. [19] for details). For the next iteration, we retain the fast bath F_n , but replace the slow bath S_n by a new site $n + 1$ coupled to new baths S_{n+1} and F_{n+1} , etc. This leads to replacing \mathcal{H} by $\mathcal{H}_N^{\text{OWC}} = \mathcal{H}_N^{\text{SWC}} + \mathcal{H}_N^{\text{TBM}}$, with

$$\begin{aligned} \mathcal{H}_N^{\text{SWC}} &= \mathcal{H}_f^{\text{imp}} + \sum_{n=0}^N \varepsilon_n f_n^\dagger f_n + \sum_{n=0}^{N-1} (f_{n+1}^\dagger t_n^S f_n + \text{H.c.}), \\ \mathcal{H}_N^{\text{TBM}} &= \sum_{n=0}^N (b_{F_n}^\dagger t_n^F f_n + \text{H.c.}) + \sum_{n=0}^N \mathcal{H}_n^F \\ &\quad + (b_{S_N}^\dagger t_N^S f_N + \text{H.c.}) + \mathcal{H}_N^S, \end{aligned} \quad (3)$$

and $\mathcal{H}_f^{\text{imp}} = \mathcal{H}^{\text{imp}}[f_0^\dagger t_{\text{imp}}]$. This chain Hamiltonian is depicted schematically in Fig. 1(c). $\mathcal{H}_N^{\text{SWC}}$ has the structure of a SWC, while $\mathcal{H}_N^{\text{TBM}}$ describes the couplings to all fast baths $F_{n \leq N}$, and of the last site N to its slow bath S_N . These “fast and last slow” baths F_n and S_N constitute TBMs, since a SWC neglects their influence, namely, to shift, mix, and broaden the eigenstates of those subchains to which they couple. Equation (3), which represents an impurity model in terms of a Wilson chain that

still is a fully open system, is the first main result of this Rapid Communication.

Renormalized Wilson chain. For concrete numerical calculations, we need to approximate an OWC by a RWC that can be treated using standard NRG or VMPS methods, while still including information about the TBMs. To this end, we replace \mathcal{H}^{OWC} by \mathcal{H}^{RWC} [Fig. 1(d)], a Hamiltonian of the same form as \mathcal{H}^{SWC} (without fast or last baths), but with each on-site energy ε_n shifted to

$$\tilde{\varepsilon}_n = \varepsilon_n + \delta\varepsilon_n^F + \delta_{nN} \delta\varepsilon_N^S, \quad \delta\varepsilon_n^X = \text{Re}[\Sigma_n^X(0)]. \quad (4)$$

For the CFE of $\mathcal{G}^{\text{bath}} = \mathcal{G}_{-1}^S = \mathcal{G}_0$, this amounts to replacing the slow and fast self-energies by the real parts of their zero-frequency values [21]. Therefore, $\text{Re}[\Sigma^{\text{bath}}(0)]$, the real part of the zero-frequency self-energy of $\mathcal{G}^{\text{bath}}$, is reproduced correctly [22], irrespective of the length N of the RWC used to calculate $\mathcal{G}^{\text{bath}}$. (Since the imaginary parts of all self-energies are neglected, dissipative effects are not included.) If the original bath spectrum is symmetric, $\Gamma^{\text{bath}}(\omega) = \Gamma^{\text{bath}}(-\omega)$, as often happens for fermionic models, then $\delta\varepsilon_n^{S/F} = 0$. However, for an asymmetric bath function [e.g., $\Gamma^{\text{bath}}(\omega < 0) = 0$, as is the case for bosonic baths], these shifts are in general nonzero.

We will henceforth consider two types of RWCs, labeled by C1 or C2 [23]. A C1 chain includes only fast shifts ($\delta\varepsilon_N^S = 0$); this turns out to lead to results qualitatively similar to those obtained using a SWC constructed by discretizing the original bath logarithmically, as done by Wilson, and tridiagonalizing the bath Hamiltonian $\mathcal{H}^{\text{bath}}$. A C2 chain includes both the fast and slow shifts from Eq. (4), thus correctly reproducing $\text{Re}[\Sigma^{\text{bath}}(0)]$.

Dissipative harmonic oscillator. As a first example, consider a DHO with Hamiltonian $\mathcal{H}_{\text{DHO}}^{\text{imp}} + \mathcal{H}^{\text{bath}}$, where

$$\mathcal{H}_{\text{DHO}}^{\text{imp}} = \Omega a^\dagger a + \frac{1}{2}(a + a^\dagger)[\epsilon + t_{\text{imp}}(b + b^\dagger)] \quad (5)$$

describes an ‘‘impurity’’ oscillator with bare frequency Ω and displacement force ϵ , linearly coupled to a bosonic bath. The bath spectral function has the form

$$\Gamma^{\text{bath}}(\omega) = 2\alpha\omega_c^{1-s}\omega^s, \quad 0 < \omega < \omega_c, \quad (6)$$

where $s > -1$, α characterizes the dissipation strength, and ω_c is a cutoff frequency, henceforth set to unity. This model is exactly solvable. The static impurity susceptibility at temperature T , defined by $\chi(T) = \frac{d\langle a^\dagger a \rangle_T}{d\epsilon}|_{\epsilon=0}$, turns out to be temperature independent and given by [17] $\chi_{\text{exact}}(T) = 1/\Omega_r$, where $\Omega_r = \Omega + \text{Re}[\mathcal{G}^{\text{bath}}(\omega = 0)]$ can be interpreted as the renormalized impurity frequency, reduced relative to the bare one by the coupling to the bath. It vanishes at the critical coupling $\alpha_c = s\Omega/(2\omega_c)$, beyond which the model becomes unstable.

When $\chi(T)$ is computed numerically for $\alpha < \alpha_c$ using NRG to perform thermal averages on SWCs of length N_T , one does not obtain a constant but a temperature-dependent curve [15–17]. We find the same using NRG on C1-RWCs of length N_T (Fig. 2, circles). The reason is the neglect of the TBMs associated with sites $n > N_T$: Their contribution to the renormalization shift $\text{Re}[\mathcal{G}^{\text{bath}}(\omega = 0)]$ in Ω_r is missing. The approach developed above offers a straightforward cure: We simply compute $\chi(T)$ using C2-RWCs of length N_T , thus incorporating the energy shift induced by the remaining TBMs via

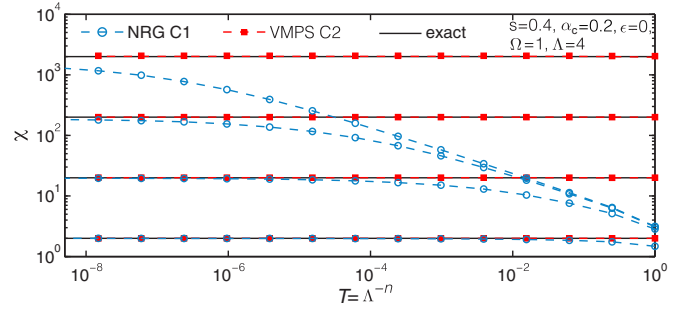


FIG. 2. DHO susceptibility $\chi(T)$ as function of temperature, computed by NRG on C1-RWCs (circles) and by VMPS on C2-RWCs (squares), for $\alpha = 0.1, 0.19, 0.199$, and 0.1999 (from bottom to top). Solid lines show exact results.

the slow-mode shift for site N_T . Since the latter substantially affects the low-energy spectrum, these calculations require VMPS methods (see Secs. S-2 B and S-2 C of Ref. [19] for details). They yield T -independent χ values (Fig. 2, squares), in excellent agreement with the exact ones (Fig. 2, solid lines).

We remark that SWCs constructed using previous discretization schemes [24–26] either strongly over- or underestimate the critical coupling α_c , reflecting the presence of discretization artifacts. In contrast, our C2-RWCs yield α_c values that match the analytic results almost perfectly (see Sec. S-3 D of Ref. [19]). Thus, our RWC construction constitutes a general, new discretization scheme free of the discretization artifacts of previous schemes.

Spin-boson model. Next, we consider the SBM, which is not exactly solvable. In its Hamiltonian $\mathcal{H}_{\text{SBM}}^{\text{imp}} + \mathcal{H}^{\text{bath}}$,

$$\mathcal{H}_{\text{SBM}}^{\text{imp}} = -\frac{1}{2}\Delta\hat{\sigma}_x + \frac{1}{2}\hat{\sigma}_z[\epsilon + t_{\text{imp}}(b + b^\dagger)] \quad (7)$$

describes a spin- $\frac{1}{2}$ ‘‘impurity’’ ($\hat{\sigma}_i$ being Pauli matrices) linearly coupled to a bosonic bath, with $\Gamma^{\text{bath}}(\omega)$ again given by Eq. (6). ϵ and Δ denote the bias and the tunnel splitting of the impurity spin, respectively.

For the *sub-Ohmic* case ($0 < s < 1$), increasing α at zero temperature drives the SBM through a quantum phase transition (QPT) from a delocalized to a localized phase (with $\langle \hat{\sigma}_z \rangle_0 = 0$ or $\neq 0$, respectively). According to a quantum-to-classical correspondence (QCC) argument [15,16,27], this QPT belongs to the same universality class as that of a classical one-dimensional Ising chain with long-ranged interactions [28]. Thus, the critical exponents characterizing the QPT follow mean-field predictions for $s \leq 0.5$ and obey hyperscaling for $0.5 < s < 1$. The QCC predictions were confirmed numerically using Monte Carlo methods [29] or sparse polynomial bases [30].

In contrast, verifying the QCC predictions using NRG turned out to be challenging. Initial NRG studies [15] yielded non-mean-field exponents for $s < 0.5$, but were subsequently [16,17] found to be unreliable, due to two inherent limitations of NRG. The first was a too severe NRG truncation of Hilbert space in the localized phase; it was overcome in Ref. [6] by using a VMPS approach involving an optimized boson basis [31–33] on a SWC, which reproduced QCC predictions for critical exponents characterizing zero-temperature behavior. The second NRG limitation was the mass-flow problem:

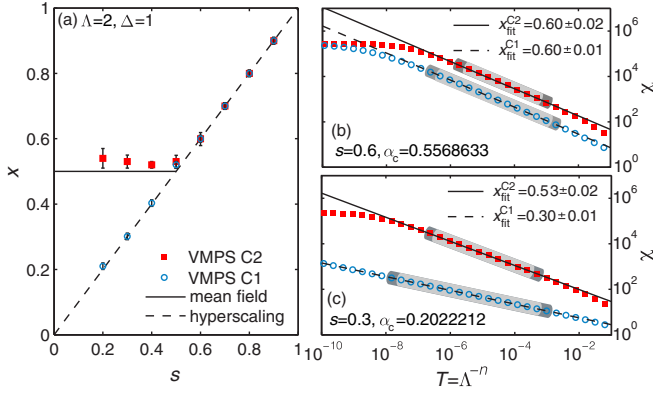


FIG. 3. (a) Critical exponent x for the sub-Ohmic SBM, as a function of s , computed by VMPS using RWCs of type C1 (circles) and C2 (squares). Examples of $\chi(T)$ curves used to extract these exponents are shown in (b) for $s = 0.3$ and (c) for $s = 0.6$. Error bars in (a) are derived by varying the fitting ranges, e.g., as indicated by dark and light shading in (b) and (c).

For exponents describing *finite*-temperature critical behavior at $\alpha = \alpha_c$, it causes NRG on SWCs to yield hyperscaling results not only for $0.5 < s < 1$ (correct) but also for $s < 0.5$ (incorrect). For example, consider the susceptibility $\chi(T) = \frac{d\langle \hat{\sigma}_z \rangle_T}{d\epsilon} \Big|_{\epsilon=0}$, which scales as $\chi(T) \propto T^{-x}$ at the critical coupling α_c . The QCC predicts $x = 0.5$ for $s < 0.5$ and $x = s$ for $0.5 < s < 1$. In contrast, past NRG calculations yielded $x = s$ throughout the interval $0 < s < 1$ [16,17,24]. We recover the latter behavior if we compute $\chi(T)$ via VMPS calculations on length- N_T C1-RWCs [Fig. 3(a), circles]. In contrast, if we use length- N_T C2-RWCs instead, the results for x [Fig. 3(a), squares] agree well with QCC predictions, showing that the mass-flow problem has been cured.

Critical energy-level flow diagrams. The reason why the sub-Ohmic SBM shows qualitatively different critical behavior for $0.5 < s < 1$ and $s \leq 0.5$ is that the critical fixed point is interacting for the former but Gaussian for the latter [17]. To elucidate the difference, Fig. 4 shows energy-level flow diagrams, obtained by plotting the rescaled lowest-

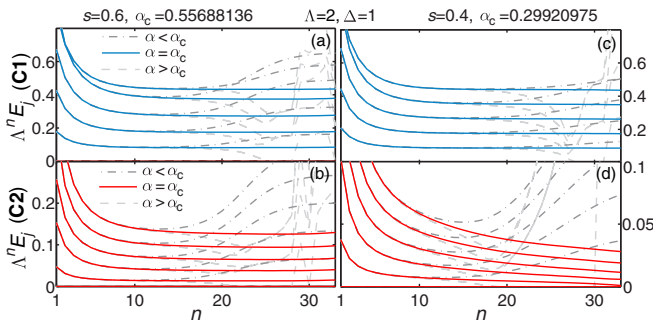


FIG. 4. Energy-level flow diagrams for the sub-Ohmic SBM with $s = 0.6$ (left column) and $s = 0.4$ (right column), computed by VMPS techniques [5,19] on C1-RWCs (top row) and C2-RWCs (bottom row). Dashed lines depict flow to delocalized ($\alpha < \alpha_c$) or localized fixed points ($\alpha > \alpha_c$), and solid lines depict critical flow ($\alpha = \alpha_c$). For the latter, the C2 flow in (d) is characteristic of a Gaussian fixed point.

lying energy eigenvalues of length- N Wilson chains, $\Lambda^N E_j$, as functions of N . For $s = 0.6$ (left column), having an interacting critical fixed point for which mass-flow effects are not relevant, the critical level flows for RWCs of type C1 and C2 are qualitatively similar [Figs. 4(a) and 4(b)], becoming stationary independent of N for large N , in a manner familiar from fermionic NRG.

In contrast, for $s = 0.4$ (right column), having a Gaussian fixed point for which mass-flow effects do matter, the critical C1 and C2 level flows are very different: Whereas the C1 flow becomes stationary [Fig. 4(c)] (an artifact of neglecting slow-mode shifts), the low-lying C2 levels all flow towards zero [Fig. 4(d)], causing the level spacing to decrease towards zero, too. This striking behavior, inaccessible when using SWCs, is characteristic of a Gaussian fixed point: It implies that the fixed-point excitation spectrum contains a zero-energy bosonic mode. Remarkably, our C2-RWCs yield a *quantitatively* correct description of the critical spectral flow for $0 < s < 0.5$: It follows a power law $\Lambda^n E_j \propto \epsilon_n^\kappa$ with $\kappa = (2s - 1)/3$, in perfect agreement with the prediction from controlled perturbative RG for a ϕ^4 -type theory with a dangerously irrelevant quartic coupling (see Sec. S-4 D of Ref. [19]).

Conclusions and outlook. Open Wilson chains are representations of quantum impurity models that achieve energy-scale separation while fully keeping track of the effects of bath modes, by iteratively replacing them by a sequence of separate baths at successively lower-energy scales, one for each chain site. Starting from such a fully open system, the effects of these baths can be included systematically. We have taken the first step in that direction, using the bath-induced energy shift for each site to define a renormalized Wilson chain. Remarkably, this simple scheme is sufficiently accurate to yield renormalized impurity properties free from the long-standing mass flow problem. The next step, namely, integrating out each site's bath more carefully, should lead to a description of dissipative effects on Wilson chains, as required for nonequilibrium situations. For example, the effect of bath F_n on the eigenstates of a length- n subchain could be treated using some simple approximation capable of mixing and broadening the eigenlevels (e.g., an equation-of-motion approach with a decoupling scheme). This is left for future work.

Finally, we note that our iterative construction of renormalized Wilson chains constitutes a well-controlled new discretization scheme that offers progress on two further fronts, unrelated to finite-size effects but relevant, e.g., when using NRG or DMRG as impurity solvers for dynamical mean-field theory [9–11,34], or to study multi-impurity models [35]. First, it avoids the discretization artifacts known to arise when conventional schemes [1,24–26] are used to treat strongly asymmetric bath spectra. Second, it can be generalized straightforwardly to treat multiflavor models having nondiagonal bath spectral functions (see Sec. S-1 B of Ref. [19]).

Acknowledgments. We thank Andrew Mitchell for a stimulating discussion on discretizing multiflavor impurity models. This research was supported by the DFG through the Excellence Cluster “Nanosystems Initiative Munich”, SFB/TR 12, SFB 631, SFB 1143 (M.V.), AN 275/8-1 (F.B.A.), and WE4819/2-1 (A.W.).

- [1] K. G. Wilson, *Rev. Mod. Phys.* **47**, 773 (1975).
- [2] R. Bulla, T. A. Costi, and T. Pruschke, *Rev. Mod. Phys.* **80**, 395 (2008).
- [3] H. Saberi, A. Weichselbaum, and J. von Delft, *Phys. Rev. B* **78**, 035124 (2008).
- [4] A. Weichselbaum, F. Verstraete, U. Schollwöck, J. I. Cirac, and J. von Delft, *Phys. Rev. B* **80**, 165117 (2009).
- [5] I. Pizorn and F. Verstraete, *Phys. Rev. Lett.* **108**, 067202 (2012).
- [6] C. Guo, A. Weichselbaum, J. von Delft, and M. Vojta, *Phys. Rev. Lett.* **108**, 160401 (2012); B. Bruognolo, A. Weichselbaum, C. Guo, J. von Delft, I. Schneider, and M. Vojta, *Phys. Rev. B* **90**, 245130 (2014).
- [7] L. Borda, G. Zaránd, W. Hofstetter, B. I. Halperin, and J. von Delft, *Phys. Rev. Lett.* **90**, 026602 (2003).
- [8] A. V. Kretinin, H. Shtrikman, D. Goldhaber-Gordon, M. Hanl, A. Weichselbaum, J. von Delft, T. A. Costi, and D. Mahalu, *Phys. Rev. B* **84**, 245316 (2011).
- [9] R. Bulla, *Phys. Rev. Lett.* **83**, 136 (1999).
- [10] T. Pruschke and R. Bulla, *Eur. Phys. J. B* **44**, 217 (2005).
- [11] K. M. Stadler, Z. P. Yin, J. von Delft, G. Kotliar, and A. Weichselbaum, *Phys. Rev. Lett.* **115**, 136401 (2015).
- [12] A. Rosch, *Eur. Phys. J. B* **85**, 6 (2012).
- [13] F. B. Anders, *J. Phys.: Condens. Matter* **20**, 195216 (2008).
- [14] F. B. Anders and A. Schiller, *Phys. Rev. Lett.* **95**, 196801 (2005). H. E. Türeci, M. Hanl, M. Claassen, A. Weichselbaum, T. Hecht, B. Braunecker, A. Govorov, L. Glazman, A. İmamoğlu, and J. von Delft, *ibid.* **106**, 107402 (2011); C. Latta, F. Haupt, M. Hanl, A. Weichselbaum, M. Claassen, P. Fallahi, S. Faelt, L. Glazman, J. von Delft, H. E. Türeci, and A. İmamoğlu, *Nature (London)* **474**, 627 (2011).
- [15] M. Vojta, N.-H. Tong, and R. Bulla, *Phys. Rev. Lett.* **94**, 070604 (2005).
- [16] M. Vojta, N.-H. Tong, and R. Bulla, *Phys. Rev. Lett.* **102**, 249904(E) (2009).
- [17] M. Vojta, R. Bulla, F. Güttge, and F. Anders, *Phys. Rev. B* **81**, 075122 (2010).
- [18] G. Grosso and G. P. Parravicini, *Adv. Chem. Phys.* **62**, 81 (2007); M. Foulkes and R. Haydock, *J. Phys. C* **19**, 6573 (1986); E. R. Gagliano and C. A. Balseiro, *Phys. Rev. Lett.* **59**, 2999 (1987); Q. Si, M. J. Rozenberg, G. Kotliar, and A. E. Ruckenstein, *ibid.* **72**, 2761 (1994); K. A. Hallberg, *Phys. Rev. B* **52**, R9827(R) (1995).
- [19] See Supplemental Material at <http://link.aps.org/supplemental/10.1103/PhysRevB.95.121115>, which includes Refs. [36–42], for details about the OWC construction, numerical methods used, and additional numerical data.
- [20] If $\Gamma^{\text{bath}}(\omega)$ has power-law form $\propto \omega^s$, we can achieve this by taking the support of \mathcal{A}_n^S and \mathcal{A}_n^F to *partition* that of $-\frac{1}{\pi}\text{Im}\Sigma_n$ into low- and high-energy regimes [19].
- [21] This choice of $\delta\varepsilon_n^X$ aims to correctly describe low-energy properties, in order to solve the mass-flow problem. More generally, the $\delta\varepsilon_n^X$ may be viewed as fit parameters that optimize the truncated CFE representation of $\mathcal{G}^{\text{bath}}(\omega)$.
- [22] For the single-impurity Anderson model, this guarantees that the height of the zero-temperature Kondo resonance at $\omega = 0$, which is governed solely by $\text{Re}[\Sigma^{\text{bath}}(0)]$, is reproduced correctly, irrespective of the choice of Λ .
- [23] Chains that include neither fast nor slow shifts, $\delta\varepsilon_n^{F,S} = 0$, yield completely incorrect results; see Sec. S-3 of Ref. [19].
- [24] R. Bulla, N.-H. Tong, and M. Vojta, *Phys. Rev. Lett.* **91**, 170601 (2003); R. Bulla, H.-J. Lee, N.-H. Tong, and M. Vojta, *Phys. Rev. B* **71**, 045122 (2005).
- [25] V. L. Campo Jr. and L. N. Oliveira, *Phys. Rev. B* **72**, 104432 (2005).
- [26] R. Žitko and T. Pruschke, *Phys. Rev. B* **79**, 085106 (2009).
- [27] M. Vojta, *Phys. Rev. B* **85**, 115113 (2012).
- [28] M. E. Fisher, S.-k. Ma, and B. G. Nickel, *Phys. Rev. Lett.* **29**, 917 (1972); E. Luijten and H. W. J. Blöte, *Phys. Rev. B* **56**, 8945 (1997).
- [29] A. Winter, H. Rieger, M. Vojta, and R. Bulla, *Phys. Rev. Lett.* **102**, 030601 (2009).
- [30] A. Alvermann and H. Fehske, *Phys. Rev. Lett.* **102**, 150601 (2009).
- [31] C. Zhang, E. Jeckelmann, and S. R. White, *Phys. Rev. Lett.* **80**, 2661 (1998).
- [32] A. Weiße, H. Fehske, G. Wellein, and A. R. Bishop, *Phys. Rev. B* **62**, R747 (2000).
- [33] Y. Nishiyama, *Eur. Phys. J. B* **12**, 547 (1999).
- [34] F. A. Wolf, A. Go, I. P. McCulloch, A. J. Millis, and U. Schollwöck, *Phys. Rev. X* **5**, 041032 (2015).
- [35] A. K. Mitchell and R. Bulla, *Phys. Rev. B* **92**, 155101 (2015); A. K. Mitchell, P. G. Derry, and D. E. Logan, *ibid.* **91**, 235127 (2015).
- [36] A. Weichselbaum and J. von Delft, *Phys. Rev. Lett.* **99**, 076402 (2007).
- [37] L. Borda, *Phys. Rev. B* **75**, 041307 (2007); B. Lechtenberg and F. B. Anders, *ibid.* **90**, 045117 (2014).
- [38] S. R. White, *Phys. Rev. Lett.* **69**, 2863 (1992); *Phys. Rev. B* **48**, 10345 (1993); U. Schollwöck, *Rev. Mod. Phys.* **77**, 259 (2005).
- [39] U. Schollwöck, *Ann. Phys.* **326**, 96 (2011).
- [40] C. Brockt, F. Dorfner, L. Vidmar, F. Heidrich-Meisner, and E. Jeckelmann, *Phys. Rev. B* **92**, 241106 (2015); F. A. Y. N. Schröder and A. W. Chin, *ibid.* **93**, 075105 (2016); F. Dorfner and F. Heidrich-Meisner, *Phys. Rev. A* **93**, 063624 (2016).
- [41] N.-O. Linden, Master's thesis, LMU Munich, 2014.
- [42] H.-J. Lee, R. Bulla, and M. Vojta, *J. Phys.: Condens. Matter* **17**, 6935 (2005).